

Estimating Silent Data Corruption Rates Using a Two-Level Model

Siva Kumar Sastry Hari¹, Paolo Rech², Timothy Tsai¹, Mark Stephenson¹, Arslan Zulfiqar¹, Michael Sullivan¹, Philip Shirvani, Paul Racunas¹, Joel Emer¹, Stephen W. Keckler¹

¹NVIDIA Corporation, ²Federal University of Rio Grande do Sul

ABSTRACT

High-performance and safety-critical system architects must accurately evaluate the application-level silent data corruption (SDC) rates of processors to soft errors. Such an evaluation requires error propagation all the way from particle strikes on low-level state up to the program output. Existing approaches that rely on low-level simulations with fault injection cannot evaluate full applications because of their slow speeds, while application-level accelerated fault testing in accelerated particle beams is often impractical. We present a new two-level methodology for application resilience evaluation that overcomes these challenges. The proposed approach decomposes application failure rate estimation into: (1) identifying how particle strikes in low-level unprotected state manifest at the architecture-level, and (2) measuring how such architecture-level manifestations propagate to the program output. We demonstrate the effectiveness of this approach on GPU architectures. We also show that using just one of the two steps can overestimate SDC rates and produce different trends—the composition of the two is needed for accurate reliability modeling.

1. INTRODUCTION

Transient hardware faults caused by high-energy particle strikes are of rising concern for processors deployed in high-performance computing systems and safety-critical embedded systems. These transient faults can propagate to the application level and cause execution failures, also known as Detected Unrecoverable Errors (DUEs), or worse they can silently corrupt the application output and lead to Silent Data Corruption (SDC).

The SDC rate of a system is fundamentally architecture and application dependent. Despite this cross-layer complexity, system and software architects for high-performance or safety-critical systems must ensure that the applications running on their systems achieve acceptable SDC rates. Furthermore, software developers also want to gain insight into why their applications produce certain SDC rates, if these rates are unacceptable, and how to ensure that their applications are reliable with minimal impact on performance and power.

These objectives necessitate a fast and accurate resilience evaluation technique. Quantifying how particle

strikes in unprotected low-level state propagate to the application output requires a detailed design such that transient bit-flips in unprotected structures can accurately be injected or modeled and a fast evaluation framework that propagates such low-level errors all the way to the program output, and not just to the output of a chip or a kernel. Meeting these conflicting requirements makes application SDC rate estimation challenging.

Existing approaches are insufficient to investigate application-level resilience at the level of detail required to enable software architects to quantify the SDC rates of their applications and to develop insights into what makes their applications vulnerable—insights that are key for developing low-cost resilience solutions. We categorize existing approaches into five following groups. Table 1 compares these approaches based on their speed, accuracy, complexity, and visibility into the application state corruption.

- **Low-level simulation-based fault injection** uses either an RTL-level or microarchitecture-level simulator to inject faults by flipping bits in low-level state [1, 2]. The accuracy of this approach is limited by the fidelity of its model—RTL is very accurate, microarchitecture simulators less so—and it can only study the impact of faults at the architecture- or chip-level due to slow simulation speed. Since error manifestations at these levels may not propagate to the application output, full-application analysis is impractical with this approach. FPGA-based simulations [3, 4, 5] are faster but they suffer from high implementation complexity, limited visibility into application-level error propagation, and limited availability of FPGAs that can fit chip designs that contain 10s of billions of transistors.
- **Higher-level simulation-based fault injection** either injects faults at the architecture-level or into compiler-level intermediate representations [6, 7, 8, 9, 10]. This approach is fast and provides visibility into application corruption. The error modeling accuracy, however, depends entirely on the chosen model, and it is often limited to injecting single bit-flips uniformly at the instruction-level.
- **Hierarchical fault simulations** integrate low- and higher-level simulators such that only the required details are modeled at the low-level to accurately inject

Table 1: A comparison of the various techniques for deriving application-level SDC rates.

	Low-level fault simulation		Higher-level fault injection	Hierarchical fault simulations	Microarchitecture-level ACE analysis	Accelerated fault testing	Our approach
	RTL	FPGA-based					
Captures application-level error propagation	No	Yes	Yes	Yes	Somewhat	Yes	Yes
Visibility into application state corruption	Low	Moderate	High	High	Moderate	Low	High
Fault model accuracy	High	High	Low	High	Depends on the model	High	High
Speed	Slow	Medium	Fast	Medium	Medium	Fast	Fast
Implementation complexity	Medium	High	Low	High	High	Low	Low

the fault. Once the error manifests at the higher-level, the faster simulator takes over [11, 12, 13]. While this approach is much faster than low-level simulations, the integration complexity makes it impractical for large systems.

- **Microarchitecture-level analysis** attempts to identify which values in microarchitecture structures can possibly affect correct program execution (also known as ACE analysis) [14, 15, 16, 17]. This analysis only covers structures whose occupancy can be reasoned about (e.g., large SRAM structures). As these approaches typically rely on simulation to characterize occupancy, examining full applications is prohibitively expensive.
- **Accelerated fault testing** subjects an existing chip to a high-energy particle beam and measures the observed chip error and failure rates [18, 19]. While this approach simulates the long-term behavior of computing systems and can be performed on full applications at speed, it does not allow for controlled injection or the detailed observability of errors. It also does not provide any insight into the vulnerability of low-level structures.

To enable fast, accurate, and flexible application-level error analysis, we propose a novel two-level technique that decomposes application failure rate estimation into two decoupled components: (1) identifying and modeling how particle strikes in low-level unprotected state manifest at the architecture-level, and (2) measuring how such architectural manifestations propagate to the program output. In this paper, we develop tools that enable this approach to be applied to the NVIDIA GPUs.

For the first step, we employ accelerated neutron beam testing using carefully crafted test programs on existing silicon as this methodology offers realistic fault models for accurate failure rate estimates. Each test program repeatedly executes a specific instruction type and captures architecture-level error manifestation rate from the particle strikes in unprotected structures (latches, flip-flops, and SRAMs) of the systolic instruction execution pipelines. For throughput oriented processors such as GPUs, such structures are expected to be the biggest contributor to SDCs (our results also support this expectation) [20, 21]. While beam experiments are subject to statistical uncertainty, they eliminate the modeling inaccuracies that arise in simulation-based approaches. Capturing architecture-level error manifestations after

every instruction is challenging as the error checking and recording logic after every instruction can be prohibitive. We address this challenge and present methods to prepare tests for different instruction types. We call this step *Implementation-level Propagation Analysis (IPA)*.

The second step employs fast error injection into the architectural state of a program running on existing hardware and measures how these errors propagate to the program output. This propagation is a function of the program itself rather than the microarchitecture it runs on. For our GPU case study, we employed SASSIFI that instruments a CUDA program with code that can flip bits in low-level GPU assembly instruction (SASS) outputs [6]. As SASSIFI runs directly on the GPU, it is orders of magnitude faster than detailed simulators and can use unmodified applications. We call this step *Architecture-level Propagation Analysis (APA)*.

In the final step, we estimate an application’s SDC rate by combining the results from IPA and APA along with application- and device-specific performance metrics. The following are the contributions of this paper.

- A two-level methodology to estimate SDC rates that is faster than low-level simulation-based approaches, more accurate than higher-level simulations, and more flexible than accelerated application fault testing. This approach requires performing IPA experiments just once per GPU generation and fast APA experiments per application to derive application SDC rate estimates on a target GPU.
- We quantify how particle strikes in low-level unprotected structures of state-of-the-art GPUs manifest at the architecture-level using accelerated beam experiments. We address the challenge of capturing architecture-level error manifestations after every SASS instruction with minimal error checking and recording logic (by introducing it only after a long sequence of target SASS instruction).
- We estimate SDC rates of all workloads from the Rodinia benchmark suite [22] and two DOE mini-apps (CoMD [23] and Lulesh [24]). We compare these estimates to direct beam test results for a selected set of workloads.
- We present insights into how IPA- or APA-only approaches can provide inaccurate SDC rates and trends. They overestimate SDC rates and show different trends—the composition of the two is needed for accurate reliability modeling.

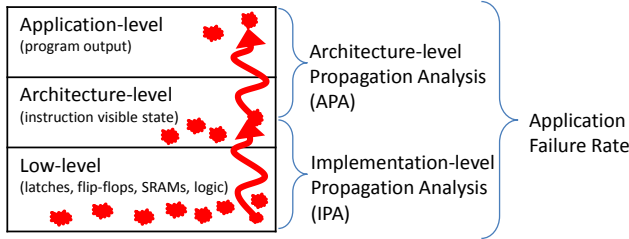


Figure 1: Composing low-level and architecture-level error propagation analyses to estimate application-level failure rate. The red symbols represent faults/errors at different levels of the design hierarchy.

2. OVERVIEW

Considering the need for a fast, accurate, and flexible application resilience analysis and the challenges associated with prior solutions (as discussed above and in Table 1), we propose a two-level application failure rate evaluation methodology that accounts for both low-level and program-level error propagation. The first step, IPA, evaluates how particle strikes in unprotected structures manifest as changes to the architecture-level state. The second step, APA, evaluates how such manifestations propagate to the program output. As a final step, we combine the results from these two steps along with simple application- and device-specific metrics to estimate application SDC rate. This rate is expressed as Failures In Time (FIT), where one FIT equals one failure in a billion hours. Figure 1 summarizes our approach. While this approach can be applied to any processor, we demonstrate it on NVIDIA GPUs.

2.1 Error Model to Bridge IPA and APA

We bridge IPA and APA with an architecture-level error model that captures bit-flips in low-level unprotected structures as bit-flips in assembly (SASS) instruction outputs. The bit-flips in low-level state can manifest in different ways at the architecture-level and the manifestation rate depends on which low-level bit is flipped. Figure 2 summarizes how we categorize low-level bits.

The vulnerability of a low-level bit is either dependent or independent of the instruction type that is executing. We call the bits whose vulnerability depends on the instruction that is executing as D-bits and the ones that do not as I-bits. For example, bits in ALU are categorized as D-bits and bits in structures that mediate communication between CPU and GPU are categorized as I-bits.

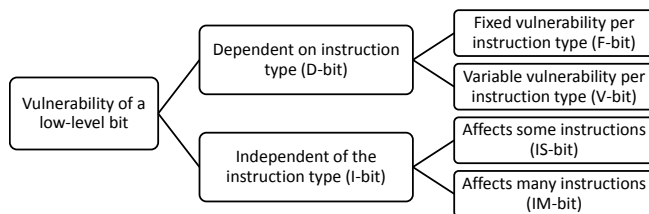


Figure 2: Categorizing low-level bits.

D-bits: Vulnerability of a D-bit can either be fixed or variable per instruction type. We call the D-bits whose vulnerability is fixed per instruction type as *F-bits*. FIT rate of these bits scales linearly with instruction issue rate. Examples of F-bits include flip-flops and SRAM bits in buffers in systolic pipeline stages. Since GPUs consist of simple in-order pipelines, bit-flips in F-bits mostly manifest as bit-flips in the destination register of one instruction in one thread.

We call the D-bits whose vulnerability varies with different microarchitecture-level buffer occupancies per instruction type as *V-bits*. FIT rate of these bits scales with instruction issue rate as well as other performance metrics. Examples of V-bits include unprotected SRAM bits in data caches, load/store buffers, and DRAM buffers. Since data can reside in these structures for a variable amount of time, the vulnerability of such bits will also vary.

Bit-flips in V-bits can manifest as DUEs or bit-flips in destination registers of instructions. For example, a bit-flip in an unprotected load buffer entry can only corrupt one instruction's output in just one thread. The size of the corruption (number of bit-flips) depends on whether the data or address bit was flipped. A bit-flip in an unprotected buffer between L2 and L1 data caches while the data is being transferred from L2 to L1 cache can manifest as a bit-flip in a cache line in L1 cache. If the cache line has only one reuse, the corruption may affect the destination registers of only one instruction. If the line has several uses, destination registers of multiple instructions in multiple threads in multiple warps can be corrupted.

I-bits: We categorize I-bits further based on the number of instructions that could be corrupted by the underlying bit-flip. We call the I-bits that corrupt only some instructions as *IS-bits* and the bits that corrupt many instructions as *IM-bits*. For example, a bit-flip in an unprotected instruction buffer in the front-end of the pipeline can corrupt the destination registers of all the threads in one warp (due to the SIMT nature of the GPUs). If the corrupted instruction is used by multiple warps then it can corrupt multiple warps. The number of instructions corrupted by this bit are, however, limited. So we call it an IS-bit. We categorize the bits that are not directly used for a specific instruction's execution, but are needed for correct functioning of the GPU as IM-bits. One example of such bits is a bit in a structure used to mediate communication between CPU and GPU. A bit-flip in it can corrupt many data words and manifest in many instructions during execution.

In this paper, we focus on modeling the impact of bit-flips in the F-bits. Our IPA results, as discussed later in Section 6.1 indicate that the F-bits are the primary sources of the SDCs. We also show the potential impact of bit-flips in the V-, IS-, and IM-bits.

We model architectural manifestations from bit-flips in F-bits using a per-instruction-type architecture-level model. For example, a particle strike in a pipeline latch while an integer add instruction is executing can propa-

gate to the destination (output) register value and corrupt just one bit location. We capture this as a single bit-flip in the destination register of the integer add instruction. We also capture the manifestations from a single event per instruction type as (1) multiple bit-flips in the destination register of one instruction, and (2) single and multiple bit-flips in the destination registers of one instruction that spans multiple threads in a warp. These error outcomes stem from our observations from IPA experiments, as discussed in Section 6.1. We use this categorization later to conduct APA experiments.

2.2 IPA

IPA can be performed in multiple ways to capture such architecture-level manifestations. Accelerated high-energy neutron beam testing using state-of-the-art GPUs, low-level (RTL) error injection based studies, and ACE analysis using detailed microarchitecture-level simulators are three such ways. While the latter two approaches can be performed in pre-silicon stages, the availability of the detailed simulation infrastructure, simulation speeds, or design complexity often become the limiting factors. We chose the first approach because (1) the phenomenon that induces errors is closest to the natural occurrences of soft errors, (2) we do not have modeling inaccuracies that simulation based approaches suffer, and (3) we do not require detailed low-level simulators. For the beam testing, we designed workloads that repeatedly execute a specific instruction per workload and capture manifestations in the outputs of each instruction. The output of this analysis is a set of error propagation rates for different manifestations (e.g., single- or double-bit flips in one destination register) for each instruction type. The manifestation may also be a program crash or hang.

2.3 APA

APA can be performed in a couple of ways such as dynamic program-level liveness analysis or software-based instruction-level error injection. We choose the second approach primarily because it can precisely measure program-level error propagation (across multiple kernels in case of GPU programs) to the output. For this step, we employ a fast instruction-level error injection tool called SASSIFI that can inject into workloads running at-scale directly on the silicon [6]. For all the error manifestations observed in IPA, we perform statistical error injection campaigns per instruction type for all our workloads and obtain application-output level propagation probabilities.

2.4 Composing IPA and APA to Estimate SDC Rate

We estimate application-level failure rates by composing the results from the IPA and APA with per-application dynamic instruction distributions and device-specific performance metrics. We compute FIT rates for both SDCs and DUEs, but focus on SDCs. We use the Equation 1 to compute the per-application SDC FIT rate for F-bits. This equation essentially multiplies the rate of manifestation of an incorrect architecture state (IAS) per

instruction type, obtained during IPA, with the probability of a SDC given such architecture-level manifestation obtained during APA. It factors the instruction distribution of the application. This result is then scaled with the application’s instruction issue rate on the specific device for F-bits to account to obtain the application FIT rate (lower the issue rate, the lower the SDC rate if other parameters do not change). Per instruction type issue rate might result in a more accurate estimate, but is hard to obtain on silicon. This formulation can be used for V- and I-bits as well, but the scaling factor will depend on other performance metrics.

$$FIT_{SDC} = \left(\sum_{n=1}^N f_n \times \left(\sum_{m=1}^M pIAS_{nm} \times pSDC_{nm} \right) \right) \times s \quad (1)$$

where

N = number of instruction types in an application

f_n = fraction of application instructions of type n

M = number of architectural error manifestations, including bit flip patterns

$pIAS_{nm}$ = rate of incorrect architectural state for a specific manifestation m for instruction type n

$pSDC_{nm}$ = probability that the manifestation m in instruction type n will result in an application-level SDC

s = application and device specific scaling factor (issueIPC in this study)

We obtain $pIAS_{nm}$ values during IPA and $pSDC_{nm}$ during APA. For the IAS that are crashes and hangs, $pSDC_{nm} = 0$. We obtain f_n and s through dynamic application profiling.

3. IPA METHODOLOGY

The goal of IPA is to address two key questions. (1) How do low-level errors in state-of-the-art GPUs manifest at the outputs of the executing instructions? For example, do particle strikes in unprotected flip-flops, latches, and SRAMs propagate as single or multiple bit flips in destination registers? Do they corrupt single or multiple instructions? How many threads do they corrupt? (2) What are the rates for different instruction-level error manifestations?

Focusing on F-bits, our approach is to capture architecture-level manifestations after each instruction while running microbenchmarks on GPUs in an accelerated high-energy neutron beam. We develop a microbenchmark suite targeting seven commonly used SASS instructions. These instructions constitute nearly half of the dynamic instruction count in our workloads (see Section 6.2 for details). We expect the vulnerability from F-bits to be significant for these instructions. Each microbenchmark captures the architecture-level manifestations of particle strikes in low-level state after virtually every instruction execution. We manually attribute the observed events to F-, V-, IS-, or IM-bits. This approach provides us an estimate of the relative contribution of different types of bits to SDCs. It allows us to measure the rates for different instruction output manifestations (e.g., single

or multiple bit flips or random values in one or multiple instructions in one or multiple threads) for the different SASS instructions.

3.1 Microbenchmark Suite to Quantify Architecture-level Error Manifestations

The challenging part in developing such microbenchmarks is to capture all instruction-level manifestations while ensuring that the checking and recording code does not significantly perturb normal execution sequence of the instruction under test. The key insight we use to overcome this challenge for arithmetic instructions is to accumulate values produced by instructions into an accumulator register. We preserve the destination registers of all the instructions until we compare the accumulator’s value to a predetermined constant to check for error manifestations. If the comparison fails then we write all the register values to host pinned memory. This allows us to identify which instruction(s) observe the manifestation and which propagate the manifested corruption. Since the number of available registers per thread is limited, we need to perform the check after a certain number of back-to-back arithmetic operations. Based on the per-thread register availability, this approach allows us to keep the checking code and recording code to <10% for our microbenchmarks.

We test with ECC on, which means the register file, L1 and L2 caches, shared memory, and DRAM are protected from single-bit flips. We record but ignore uncorrected ECC errors in this study. We develop seven microbenchmarks that target the seven commonly used SASS instructions based on dynamic instruction profile of the workloads from the Rodinia benchmark suite: IADD, FADD, IMAD, FFMA, LDS, ISETP, and BRA [25]. This mix contains integer, floating point, shared memory load, and control instructions. For each target instruction, we write a CUDA kernel such that the targeted instruction executes repeatedly to dominate the total runtime. These programs have almost no control and memory divergence. For the most part, the threads operate completely out of the register file and do not use the memory subsystem (except for the I-caches).

Arithmetic Instructions: For the IADD kernel, we first initialize the register content and then execute a long sequence of IADD instructions that executes a Fibonacci series. After the series, which is about 45 instructions long in our setup, we compare the final value with the expected value. If a mismatch is detected, we store all the register values (outputs of each of the instructions that are part of the Fibonacci series) to host memory to be logged by the host for post-processing. Figure 3 shows the main section of this program. We prepared programs for the other arithmetic instructions (FADD, IMAD, and FFMA) using a similar approach, i.e., accumulating values from a sequence of instructions to reduce interference from the checking and recording code. This approach allows us to map the every manifestation back to the instruction where it originated and how it manifested (in one or multiple instructions).

```

MOV32I R12, 0x1;           // Initial value
.LOOP_BEGIN:
  IADD R13, R12, 0x2;      // Series of add instructions
  IADD R14, R12, 0x4;
  IADD R15, R13, R14;
  IADD R16, R14, R15;
  .
  IADD R58, R56, R57;
  IADD R59, R57, R58;     // Final accumulated value
  // Check the final result with expected value
  ISETP.NE.AND P0, PT, R59, c[0x2][0x0], PT;
@P0 BRA .LOG_INFO;       // Branch out in case of a mismatch
  IADD R10, R10, 0x1;     // Loop index variable
  ISETP.LT.AND P0, PT, R10, c[0x0][0x150], PT;
@P0 BRA .LOOP_BEGIN;
.LOG_INFO:                // Log info to host-pinned memory
.
  ST.E [R6+0xf58], R10;   // Store loop index variable
  ST.E [R8+0x8], R12;     // Store all register values
  ST.E [R8+0x10], R13;
.
  ST.E [R8+0xc8], R59;

```

Figure 3: The main section of the microbenchmark that tests how particle strikes in IADD manifest at the architecture-level.

Compare Instruction: An ISETP instruction compares the input operand registers and writes the one-bit result into a predicate register. There are seven one-bit predicate registers in the Kepler ISA (our target GPU is Kepler-based) [25]. Our ISETP kernel also contains a long loop that executes a sequence of ISETP instructions with a few other instructions. We hand-modify the body of this loop such that we execute seven back-to-back ISETP instructions (that write to different predicate registers) followed by a P2R instruction;¹ this moves all seven predicate bits (along with condition codes) into a general purpose register. We accumulate the value of these general purpose registers, similar to our IADD kernel, and move them to host memory if the accumulated value does not match the expected value. This provides us the ability to map every manifestation back to the instruction where the error would have originated. We can also identify if multiple instructions in one or multiple threads manifest at a similar time. Through this approach we may attribute an error in the P2R instruction as an error in the ISETP instruction, which is one of the limitations.

Branch Instruction: For the BRA program, we write a chain of branch instructions such that the target of each branch instruction is another branch instruction. We separate these instructions by tens of instructions and insert filler branch instructions that jump to a record routine and terminate program. These filler branch instructions do not execute on a fault-free run. We execute these chained branch instruction in a loop that terminates after a certain number of iterations. The record routine logs the loop index variable and allows us to detect whether the loop terminated early. An error in the executing branch instruction can result in the following three events. (1) Control transfer to a filler instruction:

¹We use non-publicly available tools to generate and assemble this hand-modified SASS code.

The designed program will terminate early (without completing predetermined loop iterations) and record the loop index variable for post-processing. (2) Control transfer to outside the program: Program crashes in these cases. (3) Control transfers to non-filler instructions: Some of these errors can go undetected and we reduce this probability by limiting non-filler instructions.

Shared Memory Load Instruction: For the loads from shared memory (LDS), we first write known values to the all the shared memory locations. We load them to different registers in a loop iteration. We accumulate the values into an accumulator, using a similar concept as in IADD program above, and record the register content for later inspection if the accumulator does not match its expected value. In this program we can distinguish whether the IADD or the LDS instruction noticed the error as the IADD instructions should only corrupt the accumulator not the individual register. The data in shared memory is protected by ECC from direct particle strikes.

3.2 Beam Experiments

We conducted the beam experiments to quantify architectural manifestations for the arithmetic and compare instructions (IADD, IMAD, FADD, FFMA, and ISETP) at the ISIS facility near Oxford, United Kingdom and for the branch and shared memory load instructions (BRA and LDS) at the LANSCE facility at Los Alamos, New Mexico using NVIDIA K40 Tesla GPUs [26]. Figure 4 shows the K40 board and the accompanying hardware in the beam experiment room on the first day of testing at ISIS. The neutron flux at these facilities is 4-7 orders of magnitude higher than the flux at sea level. We adjusted the microbenchmark runtimes (using loop iteration counts) such that the probability of observing only one architectural-visible error (crash or value corruption) due to a particle strike is high. This allow us to scale accelerated beam test results to realistic environments. We calibrate the FIT rates obtained from different beam testing facilities based on a common test with known FIT rate.

The K40 board includes a Kepler architecture based GK110b GPU chip and 12 GB GDDR5 [27]. We irradiated just the GPU chip. The chip is fabricated using 28nm planar bulk technology from TSMC and includes 15 Streaming Multiprocessors (SMs), up to 2048 threads/SM, 30 Mbit total register file (RF), 7.86 Mbit total L1 cache/Shared memory, 12 Mbit L2 cache. The register files, shared memory, caches, and DRAM are ECC protected and we run with ECC on.

We compute the FIT rate per architectural manifestation per instruction using fluence (total number of high-energy neutrons), event counts, and New York City-level flux (13 neutrons/cm²/hour [28]). In this paper, we only show relative FIT rates. We conducted tests over several days with an effective beam time of over fifteen hours with a single GPU for these tests. The total beam usage time was higher, considering the setup and down time. The 95% confidence interval error bars for the FIT rate

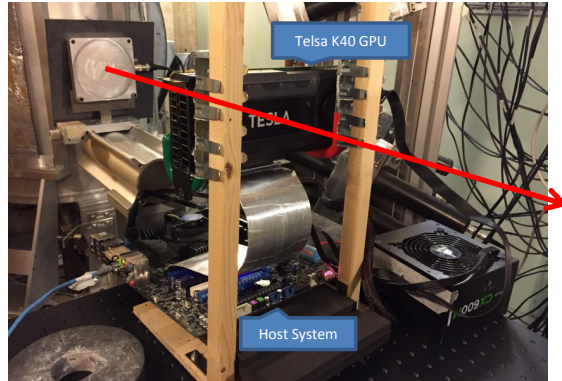


Figure 4: A picture of the experimental setup at the ISIS beam testing facility.

per microbenchmark are [42%, -29%] for IADD, [49%, -33%] for FADD, [42%, -29%] for IMAD, [38%, -27%] for FFMA, [261%, -69%] for ISETP, [40%, -28%] for BRA, and [58%, -36%] for LDS. The error bars are not tight because we used only one GPU for this campaign (parallel experiments with multiple GPUs can lower the error bars significantly). We, however, observed a variety of instruction-level manifestations including single, double, 3+ bit flips in one destination register in a single thread, double and 3+ bit flips in one destination register across the threads in a warp for different instruction types. The results are shown in Section 6.

3.3 Event Categorization and Attribution

We run our microbenchmarks back-to-back while logging state (using heartbeats) of each run at various points in the program and recording any errors that are reported by the program or system. If a program takes more than 3x its expected runtime, we terminate it and call the event a hang. If the system becomes unresponsive, we restart it. On every failure (crash or hang), we reset the GPU (using nvidia-smi tool [29]) before continuing with the next run. During program execution, we record status messages before and after the GPU kernel and flush the contents to a file, which help us to identify the failures that occur during the GPU kernel execution.

If a failure occurs before the kernel starts, we attribute it to a bit-flip in an IM-bit. If a hang is detected during a kernel execution, we have visibility in diagnosing the root cause, and cannot attribute the event to a low-level bit type. If the kernel or program crashes during kernel execution, we inspect the error code as reported by the CUDA error handler or the Linux kernel log (which we collect during LDS and BRA experiments) to attribute the error to a particular bit type. We attribute the illegal-instruction error to IS-bits because we hypothesize that a bit-flip in an unprotected buffer while fetching the instruction results in such a manifestation. We attribute the out-of-range errors and the stack errors (which occurred only during the LDS and BRA experiments, respectively) to F-bits.

On a program completion (without a crash or hang), we inspect the recorded values and compare them to

the expected values. If all the values match, we assume that either the loop control or checking logic in the microbenchmark is affected (not the targeted instructions), which triggered the recording routine. We ignore such events. On a value mismatch, we analyze the corruption and categorize it as (1) single and (2) double bit-flips in one instruction, (3) a random value error in one instruction, (4) a random value error in same instructions in two threads, (5) double bit-flips in the same instruction across all threads in one warp, (6) a random value error in the same instruction across all threads in one warp, (7) a zero value in the same instruction across all threads in one warp, or (8) a random value error in two instructions across all threads in two warps. As events 1-4 corrupt just one instruction’s output in just one or two threads, we hypothesize that the source of corruption to be a bit-flip in a pipeline element. Hence, we attribute events 1-4 to F-bits. We hypothesize that events 5-8 are caused by bit-flips in the instruction(s) because they affect all of the threads in a warp in a same way (GPUs are SIMT in nature). Event 8 might be due to a multi-bit error that spans multiple rows in an unprotected buffer. Based on this hypothesis, we attribute events 5-8 to IS-bits.

4. APA METHODOLOGY

The second step in estimating an application’s SDC FIT rate is to quantify how instruction output-level errors propagate to the application output. We used SASSIFI in this step to inject transient errors into ISA-visible state such as general purpose registers, predicate registers, and condition codes [6]. SASSIFI leverages the SASSI [30], which provides the ability to instrument instructions in the SASS code. SASSIFI injects instrumentation before and after the instructions to identify injection sites and to inject the error by modifying destination register values, respectively.

SASSIFI operates in three main steps: (1) profiling the application to identify possible error injection sites; (2) statistically selecting error injection sites for each error model; and (3) injecting errors into applications based on the selected error model and monitoring the resultant behavior. The error model is defined by the IPA.

Profiling to Identify Error Injection Sites: In the profiling step, SASSIFI collects names of static kernels and the number of times they execute during a fault-free application run to identify the error injection space. It also collects the number of dynamic instructions of each opcode and instruction type per kernel invocation.

Since we have IPA results for seven instructions, we group instructions that we expect will propagate bit-flips in low-level state to the architecture-level similarly to the ones we tested. We examine the Kepler ISA and mark the instructions that operate solely on architectural registers to be similar to either IADD, FADD, IMAD, FFMA, or ISETP. We mark several control instructions to be similar to BRA. Since instructions in a group are expected to exercise similar low-level pipeline structures, their

inherent vulnerabilities should be strongly correlated.

As an example of these groupings, we place integer maximum/minimum, shift operations, logical operations, and float-to-integer instructions in the same group as IADD. In this study, we group single and double precision floating-point operations together. Placing them in different groups with associated IPA experiments will improve the accuracy further.

Statistically Selecting Error Injection Sites: For an architecture-level error model (from IPA) and the respective instruction group, SASSIFI statistically selects hundreds of dynamic instructions among all the dynamic kernel executions as injection sites. An error injection site is a tuple consisting of the instruction group ID, architecture-level error model, static kernel name, dynamic kernel invocation ID, dynamic instruction count, seed to randomly select a destination register, and seed to select the error for injection based on the error model (e.g., location of the bit flip for a single-bit flip model). Error bars are under 3% at 95% confidence intervals for our measured SDC probability per error model and instruction type.

Error Injections Runs: We use the *Instruction Output Value (IOV)* mode in SASSIFI for this step [6], which injects errors into destination register of the selected instruction based on the chosen error model (e.g., single- or double-bit flip) and bitmask. Only one error is injected per application run. After error injection, the application is executed to completion, unless a crash or a hang is detected. The injection outcomes are categorized based on the exit status of the application, hang detection, error messages printed during execution, differences in *stdout/stderr*, and program output comparison from that of the error-free run. Crashes and hangs are categorized as *Arch DUEs*, failure symptoms as *Potential Arch DUEs*, and *stdout* or program output differences as *SDCs*. Runs with same output as the expected error free output and no error symptoms are categorized as *Masked*.

5. COMPOSING IPA AND APA

We compute SDC FIT rate estimate by composing results from IPA and APA according to Equations 1 for each of our workloads. We call this estimate *SDC TL-FIT* (TL is abbreviation for Two-Level). We use issue IPC averaged across all the kernels in an application as the scaling factor (s) in the equation. We obtain it from *issued_ipc* metric from *nvprof* [31].

While we cover most of the dynamic instructions (80% on average as shown in Section 6.2), we do not model SDC contribution from the remaining instruction types (not shown in Figure 5). Accounting for such instructions’ implementation-level and architecture-level propagation will increase the SDC TL-FIT.

We compare the TL-FIT with IPA- and APA-only estimates. The fraction of dynamic instructions covered in IPA-only and APA-only evaluations are same as that covered in our TL-SDC calculations.

Comparison with IPA-only: For the IPA-only ap-

proach, we assume that all architecture-level manifestations that corrupt instruction output registers will result in application-level SDCs. We obtain IPA-only results by using the same equation that we used to obtain TL-FIT, except that we set $pSDC_{mn} = 1$ (in Equation 1).

Comparison with APA-only: For the APA-only approach, we perform uniform architecture-level injections, which assumes that the particle strikes in unprotected low-level state manifest as single-bit flips in destination registers of executing instructions uniformly similar to several prior studies [10, 9, 7]. We obtain APA-only results by setting the values in the fourth column (single thread, single register, single bit) in Table 3 to one and zero out all other values after column two, except for FFMA and BRA. We set the fifth column value to one for FFMA. We assume that errors in BRA instructions will result in DUEs and set the third column value to one. The APA-only approach estimates the probability of SDCs per application, not the FIT rate. So we compare the normalized APA-only results with the TL-FIT rates mainly for the relative trends.

Comparison with Beam Tests: To evaluate the accuracy of our model, we beam tested four workloads to compare the SDC FIT rates with our TL-FIT rates. We tested heartwall, lavaMD, CoMD, and Lulesh. Details about the experimentation procedure is described in Section 3.2. For the experiments, we increase the input size such that the GPU kernel execution is the significant portion of the total execution time for CoMD, Lulesh, and heartwall. We consider the kernel time as well as the time spent in copying memory towards effective execution time. For lavaMD the fraction of time spent in copying memory is significant. In these experiments, we consider any indication of a failure as a DUE. For example, if we observe a non-zero exit status or an error message in the system log, which we observe using *dmesg* utility, we categorize it as a DUE. In these experiments, whenever the program output file differs from the fault-free copy and there is no indication of a failure, we categorize the run as an SDC.

6. RESULTS

In this section, we quantify how low-level errors manifest at the architecture-level (IPA) and the probability with which such manifestations propagate to the application output (APA). We show a method to compose these two results to estimate application FIT rates and compare the results with IPA- and APA-only methods, as well as to end-to-end beam tests.

6.1 IPA

Table 2 shows the relative FIT rates for different microbenchmarks (in the second column). We normalize the results to the FIT rate of IADD microbenchmark. We show the different events observed during beam tests (e.g., crashes, hangs, architectural bit-flips) and their relative rates in columns 3-5. Values in these columns sum up to the value in column 2 per row, if there is no rounding error.

Table 2: The architecture-level error manifestation rate per microbenchmark from our beam testing campaign. We normalize the results to the total FIT rate of the IADD microbenchmark.

Bit Type	Any		F	IS
Micro-benchmark	Relative FIT	Hangs & Crashes	Architectural bit-flips & crashes	Architectural bit-flips
IADD	1	0.71	0.29	
FADD	0.8	0.63	0.17	
IMAD	0.72	0.47	0.12	0.14
FFMA	0.98	0.69	0.21	0.08
LDS	0.19	0.14	0.04	0.01
ISETP	0.25	0.13	0.13	
BRA	0.19	0.17	0.02	

Table 3: The architecture-level manifestation rate per issued instruction for the F-bits. We scale the FIT rates attributed to F-bits in Table 2 with the target instruction’s issue rate to obtain FIT rate per issued instruction. These results are normalized to the per issued instruction FIT rate of IMAD.

Instruction	FIT per instruction per SM	Crashes	Architectural bit-flips			
			Single register in single thread			1 reg per thread in 2 threads
			1 bit	2 bits	3+ bits	3+ bits
IADD	0.7		0.54	0.08	0.08	
FADD	0.42		0.08	0.17	0.17	
IMAD	1		0.40	0.40	0.20	
FFMA	0.69			0.26	0.35	0.09
LDS	0.40	0.20	0.20			
ISETP	0.67		0.67			
BRA	0.21	0.21				

As explained in Section 3.3, we attribute observed events to the four types of low-level bits. We show the attribution also in the Table (in the top row). In the third column, we show failures including hangs and crashes that happened before GPU kernel started and during the kernel execution. For some of these events, we were not able to attribute to any specific type of bit. However, the majority of these events were due to crashes/hangs before the GPU kernel execution and we attribute them to IM-bits. Among all the events that were attributed to F- and IS-bits, majority of the were architectural manifestations (as bit-flips in instruction outputs) and many were due to F-bits. The observation that majority of the architectural manifestations are attributed to F-bits suggests the proposed two-level model can be accurate for application SDC rate estimation.

We next study the distribution of the events attributed to F-bits. We show the architectural manifestation rate per issued instruction in Table 3. We scale the FIT rates presented in the fourth column in Table 2 based on the instruction issue rate of the target instruction to obtain the FIT rate per issued instruction, shown in the second column in Table 3. The rates of different instruction output-level manifestations are shown in the subsequent columns. All the values after column 2 in each row sum up to the value in column 2 if there is no rounding error. These manifestations are (1) crashes, (2) single

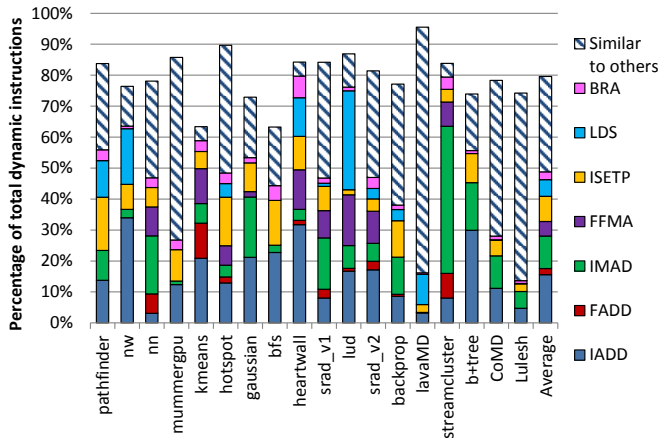


Figure 5: The fraction of different instruction types in our workloads.

bit-flips, (3) double bit-flips, and (4) 3+ bit-flips in a single register in a single thread, and (5) 3+ bit-flips in a same architectural register in two threads. We later use the absolute FIT rates (not shown here) while composing IPA and APA results. Based on these beam test results, we draw the following conclusions.

- Most of the hangs and crashes in our compute-heavy microbenchmarks are caused by the I-bits, which indicate that modeling F-bits alone is insufficient to accurately estimate the DUE rates even for the compute-heavy workloads.
- Most of manifestations that flip bits at instruction output-level are attributed to the F-bits, and these manifestations corrupt just one register in one or two threads. (1) This simplifies modeling such manifestations and quantifying their application-level propagation probabilities using APA. (2) This also implies that modeling F-bits alone for compute-heavy workloads can provide a reasonable SDC FIT rate estimate.

6.2 APA

Instruction Distribution: We plot the percentage of total dynamic instructions for IADD, FADD, IMAD, FFMA, LDS, ISETP, and BRA in Figure 5. The results show that the seven instructions represent up to 80% of the dynamic instructions (with an average of 49%) for the workloads. We also plot the percentage of dynamic instructions that we group together according to the description in Section 4. The grouping increases the representation to 80% on average for our workloads.

Architecture-level Error Injections: We conduct SASSIFI error injection campaigns for CoMD, Lulesh, and all workloads from the Rodinia benchmark suite using the error model based on the architectural manifestations observed in the IPA experiments. Specifically, we inject errors per instruction type based on Table 3. For the 3+ bit flips in a register (from Table 3) in a single register, we inject a random value in the destination register. We do not inject errors that corrupt two threads. We perform over 115,000 error injection runs, taking approximately

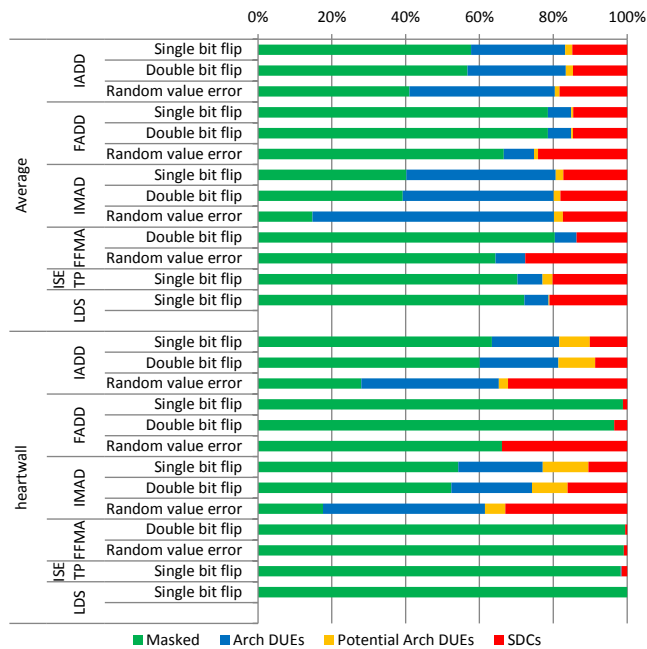


Figure 6: Masking, DUE, and SDC derating factors for different error models and opcode groups. Two results are shown: those averaged across all of our workloads and the detailed numbers for one application (heartwall).

250 hours on a Tesla K20 GPU. Note that these results do not change with the GPU, as long as the target ISA version (e.g., sm_35) is fixed. A summary of the results averaged across all the workloads is shown in Figure 6. We do not inject errors in branch instructions because we observed no events that manifest as bit-flips at the architecture-level state.

This figure, as well as the detailed per-application results (we only show heartwall here for brevity) show that injecting single and double bit flips into destination registers results in similar outcomes. We note that injecting random value errors, however, often produces different outcome distribution. Hence, it is important to know what proportion of particle strikes that manifest as 3+ bit flips in the instruction outputs. The detailed per application results show that the errors in destination registers in different instruction types behave differently. Based on these results, we draw the following conclusions, which suggest that APA is a necessary step in estimating application SDCs.

- Propagation of architecture-level error depends heavily on the application, necessitating application-specific analysis.
- Error propagation probabilities depend heavily on instruction type within an application.
- Error propagation probabilities depend on bit-flip model for a given instruction type.

6.3 SDC Rates When Composing IPA and APA

We compute SDC TL-FIT rate by composing results

Table 4: Average instruction issue rate for our workloads.

Workload	Issue IPC	Workload	Issue IPC	Workload	Issue IPC
pathfinder	2.45	nw	0.51	nn	1.26
mummergepu	1.76	kmeans	0.78	hotspot	3.49
gaussian	0.75	bfs	1.27	heartwall	1.88
srad_v1	1.69	lud	0.13	srad_v2	2.61
backprop	1.56	lavaMD	3.85	streamcluster	0.75
b+tree	1.40	CoMD	2.81	Lulesh	1.62

from IPA and APA as described in Section 5 and Equations 1. We show issue IPCs (scaling factor) in Table 4. High issue IPC for a workload implies that it is able to keep the GPU pipelines busy and has a high potential for high TL-SDC.

SDC TL-FIT rates computed using our method are shown in Figure 7 for different applications, normalized to the SDC TL-FIT rate of hotspot. We observe that either low APA SDC probabilities or issue IPC implies that the SDC TL-FIT will be low. Results show that lud, backprop, streamcluster, and Lulesh have low SDC TL-FIT rates and they all have low APA SDC probabilities. Hotspot and srad_v2 are the two applications with the highest SDC TL-FIT rates and they both have high APA SDC probabilities and average issue IPC. We next compare our results with two approaches that either do not consider IPA or APA and explain the differences. We call them APA-only and IPA-only, respectively.

Comparison with IPA-only: IPA-only approach conservatively assumes that all architecture-level manifestations will result in application-level SDCs. We show the results in Figure 7, which are normalized to the TL-FIT of hotspot. As expected, the results show that the IPA-only FIT rates are always higher than TL-FIT rates. They are, in fact, $>10x$ higher for six of our workloads. The IPA-only results also show significant differences in the trends compared to TL-FIT. For the workloads with low APA-only SDC probabilities, the difference between the TL-FIT and IPA-only FIT rates are higher. These results highlight the importance of performing IPA to quantify the architecture-level error manifestation rates and APA to quantify the application-level error propagation probabilities.

Comparison with APA-only: The APA-only approach performs uniform architecture-level injections, similar to many prior studies [10, 9, 7]. It estimates the probability of SDCs per application given an architecture-level error, not the FIT rate, making it difficult to directly compare with SDC TL-FIT. We however compare the normalized SDC probabilities in Figure 7. We normalize the applications’ SDC probabilities to the highest observed SDC probability (0.43 for srad_v2).

The results show significant differences in the trends compared to TL-FIT. For example, the top two SDC-vulnerable applications according to APA-only results have similar SDC probabilities, whereas the TL-FIT rates show a difference of nearly 1.5x. Two of the top five SDC-vulnerable applications are different when selected using the two evaluation techniques. Primary reasons for these differences are the following. (1) The TL-FIT uses abso-

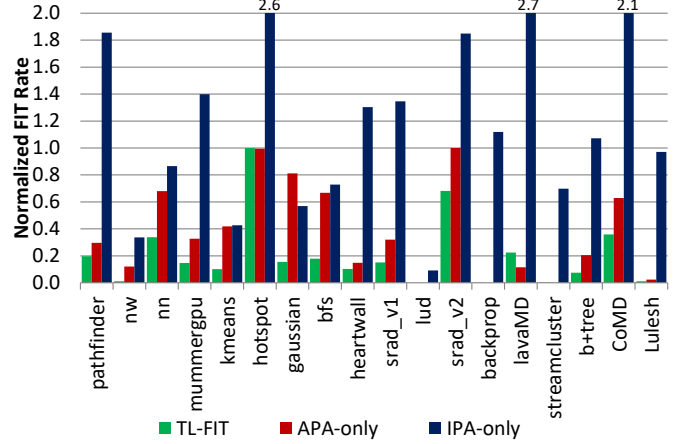


Figure 7: Relative SDC FIT rate estimates (TL-FIT) for the F-bits obtained using our compositional model. The results are normalized to the SDC TL-FIT rate of hotspot. We also show APA-only SDC probabilities and IPA-only SDC FIT rates here for comparison, which are normalized to the APA-only SDC probability of srad_v2 and the TL-FIT of hotspot, respectively.

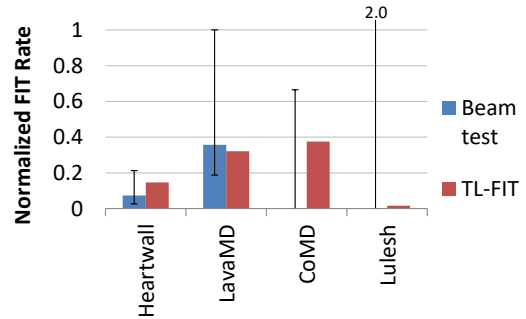


Figure 8: Comparing application SDC FIT rates obtained from direct beam tests with our TL-FIT rate estimates. SDC rates are normalized to the 95% confidence upper limit of Lulesh’s SDC FIT rates.

lute rate of architecture-level manifestations and does not rely on the accuracy of DUE estimates. The APA-only approach, however, requires the relative DUE probabilities to be accurate to estimate relative SDC probabilities. (2) The APA-only approach does not consider the relative vulnerabilities of different instructions and rates of different architecture-level manifestations. Our findings are inline with one of the prior studies (conducted on CPUs) which also showed that high-level error propagation analysis alone may be highly inaccurate when compared to studies that model errors at low-level using FPGA- or RTL-based simulators [3].

Comparison with Beam Tests: We compare SDC TL-FIT with the SDC FIT rate obtained by beam testing four workloads. The results are shown in Figure 8, which are normalized to the 95% confidence upper limit of the SDC rate of lavaMD. Results show that the SDC TL-FIT rates are close to the beam test results and are within the confidence intervals. While the error bar from

beam test measurement for Lulesh is high, we expect the SDC FIT to be low (close to 0) based on several prior studies which show that only a small fraction of low-level errors propagate to the Lulesh’s output [32, 33, 34]. Our APA results also show that only a small percentage of architectural manifestations propagate to the output, which also suggests that the SDC FIT for this application should be small compared to other workloads. A prior study showed that CoMD is significantly more susceptible than Lulesh [32]. Our SDC TL-FIT results also show the same trend.

7. DISCUSSION

7.1 Applications

Understanding Application Resilience: Identifying application characteristics that correlate well with either SDCs or DUEs is an interesting application. For example, certain programming constructs or design patterns may be associated with greater error propagation. Identification of those constructs or patterns would allow programmers to adjust their application code for higher reliability. This would also aid the development of libraries that have higher resilience, which can be substituted based on the error rate and overhead targets.

We inspected CUDA and SASS code of two workloads with highest SDC TL-FIT (hotspot and `srad_v2`), and one with least SDC TL-FIT (`lud`). For hotspot and `srad_v2`, only a small fraction of SASS instructions are used for control and address computation, whereas the fraction of instructions used for address computation is high for `lud`. These observations along with the results presented in Figure 7 indicate that whenever the fraction of instructions used for control and address computation is high, the likelihood of DUEs is also high in APA. Interestingly, prior studies have also made similar observations [35, 10]. Address randomization can be used to increase the likelihood of DUEs in the APA step.

Deciding Which Workloads Need Protection: The presented approach can be directly employed to decide which workloads need protection. For example, for an HPC system with large number of GPUs and a mean-time-to-SDC target that is usually in weeks or months, a per GPU target SDC FIT rate can be derived. This limit can be placed on Figure 7 to select applications that exceed the SDC target. As an example, with the per-GPU SDC target of 0.5 in Figure 7, we would select hotspot and `srad_v2` for protection.

Our approach can also be used to identify highly vulnerable kernels within an application to enable selective software-implemented error detection and correction methods [36, 37, 20] for cost-effective protection.

7.2 Accounting for bit-flips in IS- and V-bits

Our IPA results (Section 6.1) show that a small fraction of architecture-level bit-flip manifestations are attributed to IS-bits. These manifestations corrupt registers in multiple threads in one or two warps (categories 5-8 in Section 3.3). By definition, the rate of such manifestations

is device- and application dependent. Predicting these rates using existing performance counters is an interesting research direction. Based on our experimental data, we find inverse correlations with two performance metrics `stall_inst_fetch` and `issue_slot_utilization`, as reported by `nvprof` [31]. The correlation coefficients are -0.97 and -0.58, respectively. Developing a model to predict such manifestations would require more experiments and validation. Our APA methodology is capable of injecting these architecture-level manifestations.

The contribution of V-bits can become dominant for instructions that stress the memory subsystem (global memory loads/stores). Bit-flips in unprotected structures in the memory subsystem can propagate as bit-flips into a cache or memory line. Such a errors can corrupt a single or multiple instructions depending on the reuse characteristic of the line. We conducted IPA (beam) experiments using two microbenchmarks of load instruction that always hit and miss in L2 cache, respectively, stressing the memory subsystem in different ways. We observed higher crash/hang rate compared to the tests that focus on exercising F-bits. Interestingly, we only observed single bit flips in the destination registers of one instruction. Since the memory subsystem of GPUs has several layers of buffers, more experiments are needed to accurately model contribution of V-bits. A simulator that models some of the major unprotected buffers in the memory subsystem (e.g., SASSIFI with a detailed cache model) may be better suited to perform IPA.

7.3 Other Considerations

Our approach, as presented in the paper, is a post-silicon estimation technique because IPA and APA experiments are performed on production devices. This approach can potentially be used to estimate FIT rates of future generation GPUs by (1) scaling and extrapolating IPA results based on technology and architectural changes and (2) replacing the IPA and APA experiments with low-level pre-silicon simulation-based approaches. A prior study employed Register Transfer- and Gate-level error simulations in an out-of-order processor to quantify how low-level errors propagate to the instruction-level [2]. While this method provides high control in performing IPA, the paper focused on limited microarchitecture-level units (e.g., the scheduler and ROB). Employing such a method to more low-level units, as permitted by the available engineering resources, can be used to perform pre-silicon IPA.

We do not consider multiple-bit faults induced by particle strikes in ECC protected SRAM structures in our model because they can be converted into correctable events with an appropriate level of bit-interleaving.

Several field studies have been performed on large-scale HPC installations with thousands of GPUs [38, 39]. These studies measure the frequency of interrupts caused by GPU errors to estimate raw error and DUE rates, but not the SDC rates. Such studies are complementary to the two-level as we focus on SDC rate estimation.

8. CONCLUSIONS

This paper presents a new two-level methodology to estimate SDC rates of applications running on production GPUs. Our approach first quantifies how particle strikes in low-level unprotected state manifest at the architecture-level through accelerated beam experiments. We then perform near-silicon-speed architecture-level error injections to quantify how such manifestations propagate to the program output. Composing these two steps, which we call IPA (implementation-level analysis) and APA (architecture-level analysis), respectively, we estimated SDC rates for the workloads from Rodinia benchmark suite and two DOE mini-apps. This two-level approach allows us to estimate SDC rate of any application by performing just the APA, once the IPA is performed. IPA needs to be performed just once per GPU generation.

We compare our SDC rate estimates with accelerated beam test results for four of our workloads and find them to be close. We also compare our results with two other approaches that either perform just the IPA or APA. Results show that ignoring either IPA or APA often overestimates SDC rates and show significantly different trends—the composition of the two is needed for accurate reliability modeling.

9. REFERENCES

- [1] G. P. Saggese, N. J. Wang, Z. T. Kalbarczyk, S. J. Patel, and R. K. Iyer, “An Experimental Study of Soft Errors in Microprocessors,” *IEEE Micro*, vol. 25, no. 6, pp. 30–39, 2005.
- [2] M. Maniatakos, N. Karimi, C. Tirumurti, A. Jas, and Y. Makris, “Instruction-Level Impact Analysis of Low-Level Faults in a Modern Microprocessor Controller,” *IEEE Transactions on Computers*, vol. 60, no. 9, pp. 1260–1273, 2011.
- [3] H. Cho, S. Mirkhani, C.-Y. Cher, J. A. Abraham, and S. Mitra, “Quantitative Evaluation of Soft Error Injection Techniques for Robust System Design,” in *Proceedings of the Design Automation Conference (DAC)*, pp. 101:1–101:10, 2013.
- [4] M. Ebrahimi, A. Mohammadi, A. Ejlali, and S. G. Miremadi, “A Fast, Flexible, and Easy-to-develop FPGA-based Fault Injection Technique,” *Microelectronics Reliability*, vol. 54, pp. 1000–1008, 2014.
- [5] R. Balasubramanian and K. Sankaralingam, “Understanding the Impact of Gate-level Physical Reliability Effects on Whole Program Execution,” in *Proceedings of the International Symposium on High Performance Computer Architecture (HPCA)*, pp. 60–71, 2014.
- [6] S. K. S. Hari, T. Tsai, M. Stephenson, and S. W. Keckler, “SASSIFI: An Architecture-level Fault Injection Tool for GPU Application Resilience Evaluation,” in *Proceedings of the International Symposium on Performance Analysis of Systems and Software (ISPASS)*, pp. 249–258, 2017.
- [7] B. Fang, K. Pattabiraman, M. Ripeanu, and S. Gurumurthy, “GPU-Qin: A Methodology for Evaluating the Error Resilience of GPGPU Applications,” in *Proceedings of the International Symposium on Performance Analysis of Systems and Software (ISPASS)*, pp. 221–230, 2014.
- [8] J. Wei, A. Thomas, G. Li, and K. Pattabiraman, “Quantifying the Accuracy of High-Level Fault Injection Techniques for Hardware Faults,” in *Proceedings of the International Conference on Dependable Systems and Networks (DSN)*, pp. 375–382, 2014.
- [9] D. Li, J. S. Vetter, and W. Yu, “Classifying Soft Error Vulnerabilities in Extreme-scale Scientific Applications Using a Binary Instrumentation Tool,” in *Proceedings of the International Conference on High Performance Computing, Networking, Storage and Analysis (SC)*, pp. 1–11, 2012.
- [10] S. Feng, S. Gupta, A. Ansari, and S. Mahlke, “Shoestring: Probabilistic Soft Error Reliability on the Cheap,” in *Proceedings of the International Symposium on Architectural Support for Programming Languages and Operating Systems (ASPLOS)*, pp. 385–396, 2010.
- [11] G. Choi, R. Iyer, and V. Carreno, “FOCUS: An Experimental Environment for Validation of Fault-Tolerant Systems - Case Study of a Jet-Engine Controller,” in *Proceedings of the International Conference on Computer Design (ICCD)*, pp. 561–564, 1989.
- [12] Z. Kalbarczyk, R. K. Iyer, G. L. Ries, J. U. Patel, M. S. Lee, and Y. Xiao, “Hierarchical Simulation Approach to Accurate Fault Modeling for System Dependability Evaluation,” *IEEE Transactions on Software Engineering*, vol. 25, no. 5, pp. 619–632, 1999.
- [13] M. Li, P. Ramachandran, U. R. Karpuzcu, S. K. S. Hari, and S. V. Adve, “Accurate Microarchitecture-level Fault Modeling for Studying Hardware Faults,” *Proceedings of the International Symposium on High Performance Computer Architecture (HPCA)*, pp. 105–116, 2009.
- [14] S. S. Mukherjee, C. Weaver, J. Emer, S. K. Reinhardt, and T. Austin, “A Systematic Methodology to Compute the Architectural Vulnerability Factors for a High-Performance Microprocessor,” in *Proceedings of the International Symposium on Microarchitecture (MICRO)*, pp. 29–42, 2003.
- [15] A. Biswas, P. Racunas, R. Cheveresan, J. Emer, S. S. Mukherjee, and R. Rangan, “Computing Architectural Vulnerability Factors for Address-Based Structures,” in *Proceedings of the International Symposium on Computer Architecture (ISCA)*, pp. 532–543, 2005.
- [16] M. Li, P. Ramachandran, S. K. Sahoo, S. V. Adve, V. S. Adve, and Y. Zhou, “Understanding the Propagation of Hard Errors to Software and Implications for Resilient System Design,” in *Proceedings of the International Symposium on Architectural Support for Programming Languages and Operating Systems (ASPLOS)*, pp. 265–276, 2008.
- [17] S. Raasch, A. Biswas, J. Stephan, P. Racunas, and J. Emer, “A Fast and Accurate Analytical Technique to Compute the AVF of Sequential Bits in a Processor,” in *Proceedings of the International Symposium on Microarchitecture (MICRO)*, pp. 738–749, 2015.
- [18] J. Ziegler, H. Muhlfeld, C. Montrose, H. Curtis, T. O’Gorman, and J. Ross, “Accelerated Testing for Cosmic Soft-Error Rate,” *IBM Journal of Research and Development*, vol. 40, no. 1, pp. 51–72, 1996.
- [19] D. Oliveira, L. Pilla, T. Santini, and P. Rech, “Evaluation and Mitigation of Radiation-Induced Soft Errors in Graphics Processing Units,” *IEEE Transactions on Computers*, vol. 65, no. 3, pp. 791–804, 2015.
- [20] H. Jeon and M. Annavaram, “Warped-DMR: Light-weight Error Detection for GPGPU,” in *Proceedings of the International Symposium on Microarchitecture (MICRO)*, pp. 37–47, 2012.
- [21] M. Snir, R. W. Wisniewski, J. A. Abraham, S. V. Adve, S. Bagchi, P. Balaji, J. Belak, P. Bose, F. Cappello, B. Carlson, A. A. Chien, P. Coteus, N. A. DeBardleben, P. C. Diniz, C. Engelmann, M. Erez, S. Fazzari, A. Geist, R. Gupta, F. Johnson, S. Krishnamoorthy, S. Leyffer, D. Liberty, S. Mitra, T. Munson, R. Schreiber, J. Stearley, and E. V. Hensbergen, “Addressing Failures in Exascale Computing,” *The International Journal of High Performance Computing Applications*, vol. 28, no. 2, pp. 129–173, 2014.
- [22] S. Che, M. Boyer, J. Meng, D. Tarjan, J. W. Sheaffer, S.-H. Lee, and K. Skadron, “Rodinia: A Benchmark Suite for Heterogeneous Computing,” in *Proceedings of the International Symposium on Workload Characterization*, pp. 44–54, 2009.
- [23] Exascale Co-Design Center for Materials in Extreme Environments (ExMatEX), “CoMD: Classical Molecular

- Dynamics Proxy Application.”
<https://github.com/NVIDIA/CoMD-CUDA>.
- [24] Lawrence Livermore National Laboratory, “Livermore Unstructured Lagrangian Explicit Shock Hydrodynamics (LULESH) 2.0.”
<https://computing.llnl.gov/projects/co-design/lulesh>, 2013.
- [25] NVIDIA, “CUDA Binary Utilities :: CUDA Toolkit Documentation.” <http://docs.nvidia.com/cuda/cuda-binary-utilities/index.html#instruction-set-ref>, 2015.
- [26] NVIDIA, “Tesla K40 GPU Accelerator.”
https://computing.llnl.gov/tutorials/linux_clusters/gpu/Tesla-K40-Board-Specs.pdf, 2013.
- [27] NVIDIA, “NVIDIA’s Next Generation CUDA Compute Architecture: Kepler GK110/210.”
<https://www.nvidia.com/content/dam/en-zz/Solutions/Data-Center/documents/NVIDIA-Kepler-GK110-GK210-Architecture-Whitepaper.pdf>, 2012. Version 1.1.
- [28] JEDEC Standard, “Measurement and Reporting of Alpha Particle and Terrestrial Cosmic Ray-Induced Soft Errors in Semiconductor Devices.” <https://www.jedec.org/standards-documents/docs/jesd-89a>, 2001.
- [29] NVIDIA, “NVIDIA System Management Interface program.”
http://developer.download.nvidia.com/compute/cuda/6_0/rel/gdk/nvidia-smi.331.38.pdf, 2014.
- [30] M. Stephenson, S. K. S. Hari, Y. Lee, E. Ebrahimi, D. R. Johnson, M. O’Connor, D. Nellans, and S. W. Keckler, “Flexible Software Profiling of GPU Architectures,” in *Proceedings of the International Symposium on Computer Architecture (ISCA)*, pp. 185–197, 2015.
- [31] NVIDIA, “Profiler Users’s Guide.”
<http://docs.nvidia.com/cuda/profiler-users-guide>, 2015.
- [32] C.-K. Chang, S. Lym, N. Kelly, M. B. Sullivan, and M. Erez, “Hamartia: A Fast and Accurate Error Injection Framework,” in *Proceedings of the International Conference on Dependable Systems and Networks Workshops (DSN-W)*, pp. 101–108, 2018.
- [33] G. Li, K. Pattabiraman, S. K. S. Hari, M. Sullivan, and T. Tsai, “Modeling Soft-Error Propagation in Programs,” in *Proceedings of the International Conference on Dependable Systems and Networks (DSN)*, pp. 27–38, 2018.
- [34] B. Fang, P. Wu, Q. Guan, N. DeBardeleben, L. Monroe, S. Blanchard, Z. Chen, K. Pattabiraman, and M. Ripeanu, “SDC is in the Eye of the Beholder: A Survey and Preliminary Study,” in *IEEE/IFIP International Conference on Dependable Systems and Networks Workshop (DSN-W)*, pp. 72–76, 2016.
- [35] P. Ramachandran, S. K. S. Hari, S. V. Adve, and H. Naeimi, “Understanding When Symptom Detectors Work by Studying Data-Only Application Values,” in *Workshop on Silicon Errors in Logic-System Effects (SELSE)*, 2011.
- [36] K. S. Yim, C. Pham, M. Saleheen, Z. Kalbarczyk, and R. Iyer, “Hauber: Lightweight Silent Data Corruption Error Detector for GPGPU,” in *Proceedings of the International Symposium on Parallel and Distributed Processing (IPDPS)*, pp. 287–300, 2011.
- [37] J. Wadden, A. Lyashevsky, S. Gurumurthi, V. Sridharan, and K. Skadron, “Real-World Design and Evaluation of Compiler-Managed GPU Redundant Multithreading,” in *Proceedings of the International Symposium on Computer Architecture (ISCA)*, pp. 73–84, 2014.
- [38] C. Di Martino, Z. Kalbarczyk, R. Iyer, F. Baccanico, J. Fullop, and W. Kramer, “Lessons Learned from the Analysis of System Failures at Petascale: The Case of Blue Waters,” in *Proceedings of the International Conference on Dependable Systems and Networks (DSN)*, pp. 610–621, 2014.
- [39] D. Tiwari, S. Gupta, J. Rogers, D. Maxwell, P. Rech, S. Vazhkudai, D. Oliveira, D. Londo, N. Debardeleben, P. Navaux, L. Carro, and B. Bland, “Understanding GPU Errors on Large-scale HPC Systems and the Implications for System Design and Operation,” in *Proceedings of the International Symposium on High Performance Computer Architecture (HPCA)*, pp. 331–342, 2015.